Check for updates

L-DOPA modulates the kinetics but not the thermodynamic equilibrium of TTA$^+$ amphiphiles forming lyotropic nematic liquid crystals†

Álvaro R. Ruiz-Fernández, [ID]‡[ab] Felipe Villanelo, [ID]‡[ac] Sebastian E. Gutierrez-Maldonado, [ID][ac] Claudia Pareja-Barrueto,[ac] Boris E. Weiss-López*[b] and Tomas Perez-Acle [ID]*[acd]

Lyotropic liquid crystals (LLCs) are mixtures of amphiphile molecules usually studied as mimetic of biological membrane. The equilibrium dynamics of tetradecyltrimethyl ammonium cation (TTA$^+$) molecules forming nematic LLCs (LNLCs) is guided by a dive-in mechanism where TTA$^+$ molecules spontaneously leave and re-enter the bicelle. Of note, this dynamic behavior could be exploited to produce drug nano-delivery systems based on LNLCs. Therefore, the understanding of the effect of pharmaceutically interesting molecules in the dynamics of the dive-in mechanism should be crucial for drug delivery applications. In this work, we studied the effects of L-DOPA in the equilibrium dynamics of TTA$^+$ bicelles forming LNLCs, employing a transdisciplinary approach based on ^{2}H-NMR together with molecular modeling and molecular dynamics simulations. Our data suggest that L-DOPA perturbs the kinetic of the dive-in mechanism but not the thermodynamics of this process. As whole, our results provide fundamental insights on the mechanisms by which L-DOPA govern the equilibrium of LNLCs bicelles.

1 Introduction

Parkinson's disease (PD) is a neurodegenerative disorder characterized by continuous neuronal death producing a lack of dopamine in the *Substantia nigra* of the human brain.[1] Dopamine is a catecholamine neurotransmitter derived from L-3,4-dihydroxyphenylalanine, commonly known as L-DOPA. As a precursor of dopamine, L-DOPA has become the most used treatment for PD due to its ability to cross the blood–brain barrier, reaching the *Substantia nigra*. Despite its wide use, L-DOPA administration it is not an issue-free therapy for the treatment of PD. L-DOPA is very unstable compound. Near 99% of L-DOPA administered orally is degraded either *via* oxidation or decarboxylation.[2,3]

L-DOPA administration also produces side effects such as nausea, sleepiness and dyskinesia[4] and, due to its high metabolic clearance, maintaining a constant L-DOPA plasma concentration requires both elevated and continuous dosage, exacerbating its side effects.[5] To deal with these issues, different delivery systems have been developed including microspheres, dendrimers, and micelles for infusion and transdermal delivery.[5,6] Recently, the use of biodegradable copolymers of glycolic and lactic acids used *via* nasal L-DOPA administration, have attract the attention of many investigators[7] In recent years, mixtures of amphiphilic molecules in solutions received significant attention as potential delivery systems. Among these, solutions made of orientationally ordered discotic aggregates (bicelles[8] among others), termed as lyotropic nematic liquid crystals (LNLCs), exhibit several uses such as, to grow oriented carbon nanotubes,[9–11] to synthetize silica and metals containing regularly oriented nanopores and,[12–17] as membrane mimetics,[18–20] and as micro-lubricants.[21,22] Of note, more recently, LNLCs has been proposed as simple but versatile carriers for pharmaceutical formulations to avoid the metabolic clearance and to maintain constant plasma concentration of drugs.[23–26] Due to their geometry, bicelles have an anisotropic diamagnetic susceptibility that makes them spontaneously align in magnetic fields, with the symmetry axis of the disk perpendicular to the direction of the field. This enables the obtention of valuable experimental information such as quadrupole splittings that helps to understand its intrinsic dynamics nature. In a previous work, a mechanism for the insertion and expulsion of an amphiphile molecule from a bicelle, called the dive in mechanism, has been proposed.[27] Considering that

[a]*Computational Biology Lab, Fundación Ciencia & Vida, Santiago, Chile. E-mail: tomas@dlab.cl*

[b]*Universidad de Chile, Facultad de Ciencias, Departamento de Química, Casilla 653, Santiago, Chile. E-mail: bweiss@uchile.cl*

[c]*Centro Interdisciplinario de Neurociencia, Universidad de Valparaíso, Valparaíso, Chile*

[d]*Universidad San Sebastian, Carmen Sylva 2444, Santiago 7510156, Chile*

† Electronic supplementary information (ESI) available. See DOI: 10.1039/d0ra00764a

‡ These authors contributed equally to this work.

LNLCs could be used as delivery systems for drugs, particularly L-DOPA, we performed an experimental and theoretical study aimed to determine how the presence of L-DOPA modulates the dive in mechanism of the amphiphiles forming the LNLC. Notably, our data suggest that, while the inclusion of L-DOPA in the media actually modulates the kinetics of the dive in mechanism generating additional micro-states where several more TTA$^+$ amphiphiles could be out of the bicelle, the thermodynamics of this process, remain unaltered. Therefore, future applications of LNLC to the development of drug delivery systems, should consider the effect of the drug concentration on the dynamical behavior of bicelles.

2 Methodology

2.1 Mesophase preparation

L-DOPA was purchased from Santa Cruz Biotechnology and used as received. L-DOPA-d$_3$ was purchased from ISOTEC. Fully deuterated sodium dodecylsulphate (SDS-d$_{25}$), tetradecyltrimethyl ammonium chloride (TTAC) and decanol (DeOH) were purchased from Aldrich. HPLC-grade water and sodium chloride (NaCl) at the highest purity available were purchased from Merck. All compounds were used as received. The base solution (BS) for this study was taken from a previous work from our group.[27] It was prepared by dissolving 0.3448 g of TTAC, 0.1094 g of NaCl and 0.0730 g of DeOH in 1 ml of H$_2$O, and was equilibrated 48 hours at 300 K, before any measurements were performed. To study the effect of L-DOPA in this system three different solution were prepared. System 1: BS + 18 mg SDS-d$_{25}$ + 5 μL of D$_2$O. System 2: BS + 18 mg SDS-d$_{25}$ + 7.5 mg L-DOPA + 5 μL of D$_2$O. System 3: BS + 7.5 mg of L-DOPA-d$_3$ + 5 μL of D$_2$O. In the preparation of the three systems when SDS-d$_{25}$ and D$_2$O were included, SDS and H$_2$O were removed in the same amount to maintain the concentration of BS.

SDS-d$_{25}$ is added because it is used to test the effect of L-DOPA in the aggregate structure, following modifications in the dynamics of the aliphatic chains of SDS-d$_{25}$ at different depths towards the interior of the hydrophobic core. D$_2$O is added because $\Delta\nu_Q$ of water deuterium gives valuable information about the interface dynamics. L-DOPA-d$_3$ will provide information about the interaction of the drug with the aggregate components.

2.2 ^{2}H-NMR spectra

^{2}H-NMR spectra were obtained in a Bruker Avance 400 NMR spectrometer, located at the Universidad de Santiago de Chile, using a broadband probe tuned to 61.425 MHz, at 300 K. The ^{2}H 90° pulse was 19 μs long and more than 1000 transients from a spectral window of 40 kHz were accumulated in 32 kB files.

2.3 Polarized light microscopy (PLM)

A Motic series B microscope with crossed polarizers was employed to observe the textures. The samples were placed in a concave slide with a depth of 1 mm and were allowed to orient in a 1.4 T magnet for 15 min. The photos were taken with a 20-fold magnification, from the center of the concavity, avoiding variations in the thickness of the sample due to the curvature of the slide. Photos were obtained at 300 K.

2.4 MD simulations

2.4.1 Equilibrium MD. To conduct the theoretical study, we modeled a NPT ensemble of a bilayer section of the bicelle, containing amphiphilic proportions similar to that of the Experimental section representing the BS, as reported elsewhere.[27] A time step of 2 fs were used in all simulations. This simulation, named Box 1, satisfactorily reproduces $\Delta\nu_Q$ from SDS-d$_{25}$. As before, during the simulation, a dynamic of insertion/expulsion of TTA$^+$ molecules between the bulk and the aggregate was established.[27] To determine whether the inclusion of L-DOPA could affect the kinetic and/or equilibrium of the bicelle formed by TTA$^+$, L-DOPA molecules were added to match the experimental proportions of system 2 (see Section 2.1), generating Box 2. Box 2 contains exactly 60 TTA$^+$, 12 DeOH, 8 DS$^-$, 4 Na$^+$, 60 Cl$^-$, 2 L-DOPA and 2883 molecules of H$_2$O. A graphic representation of Box 2 is presented in Fig. 1.

Of note, SDS is a salt that in aqueous solution dissociates in its cation and anion, thus in the solution used for NMR experiments, SDS becomes dissociated in SD$^-$ and Na$^+$. Thus, the NMR results are from SD$^-$. For this reason, the MD simulation protocols used SD$^-$.

The amount of L-DOPA in system 2 is close to the saturation point, thus no additional concentration-response experiments, could be performed. However, for theoretical simulations, an increased number of L-DOPA molecules can be included.

Therefore an additional simulation containing exactly the same molecules as Box 1, but adding four L-DOPA molecules was generated and named Box 3. Thus Box one is basically a bilayer of TTA$^+$, and; Box 2: is Box 1 + 2 L-DOPA and Box 3: is Box 1 + 4 L-DOPA. Atomic charges of all simulated molecules are
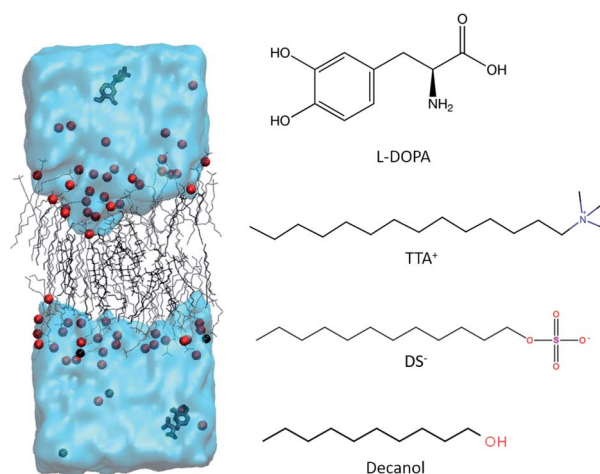

Fig. 1 Molecular models used in this study. Panel left, representation of simulation Box 2. The cyan blob represents water, spheres in red and black represent Cl$^-$ and Na$^+$ ions, respectively. L-DOPA appears rendered using black sticks in water, and at the center of the simulation box appear the components of the bicelle; TTA$^+$ amphiphiles, DeOH and DS$^-$, all rendered using sticks. Right panel, 2D structures of L-DOPA, TTA$^+$, DS$^-$ and DeOH.

presented in Table S3† along with Fig. S6.† The equilibrium condition reached by the simulations, studied specifically for Box 3, is presented in Fig. S4 and S5.†

2.4.2 Steered MD. Steered MD (SMD) simulations were performed to analyze the putative thermodynamic effects of L-DOPA in the TTA$^+$ insertion/expulsion mechanism. The simulation of the insertion/expulsion process of one TTA$^+$ molecule was performed using the Gromacs 5.1.4 molecular dynamics engine patched with Plumed version 2.3.[28] A distance restraint protocol was used, defining the reaction coordinate as the distance along the z-axis between one atom of TTA$^+$ and the average of the corresponding atoms of the rest of the TTA$^+$ molecules in the closer monolayer. The TTA$^+$ atoms used for steering were nitrogen for expulsion, and the last carbon of the tail for insertion. The protocol followed was: (i) reach a zero distance in 120 ps; (ii) hold zero distance for 40 ps; (iii) apply a force to drag the TTA$^+$ molecule with a constant velocity, from zero distance to the maximum distance (4 nm) in 740 ps; (iv) hold the TTA$^+$ position in the maximum distance for 100 ps. The time step used here is the same used in Equilibrium MD (2 fs). In the step (iii) the pulling of the TTA$^+$ molecule reach a velocity of 0.05 Å ps^{-1}. During all the applied protocols a spring constant of 1000 kJ mol^{-1} nm^{-2} was used. The force exerted at step (iii) was extracted for further statistical analysis. Other simulation conditions were the same as described above. The insertion and expulsion was performed for 8 TTA$^+$ molecules. We repeated this protocol three times per steered molecule to collect enough data to compute statistics, generating a total of 48 independent simulations for the total of the insertion and expulsion events. A distance restraint of 1 nm between the L-DOPA center of mass and the center of mass of all nitrogen in the bilayer was applied with a spring constant of 100 kJ mol^{-1} nm^{-2}. An angle restriction was applied to keep an angle of zero between the bilayer surface and the aromatic ring of L-DOPA, with a spring constant of 100 kJ mol^{-1} nm^{-2}.

3 Results and discussion

3.1 Experimental data, ^{2}H-NMR and PLM

^{2}H-NMR spectra of the three studied systems (see Section 2.1) with their PLM textures are shown in Fig. 2. The spectra profile and the textures observed in PLM correspond to Schlieren textures, confirming that the three systems are in the same lyotropic nematic phase.[29–34] The Schlieren texture is the name given to the colored texture observed when a polarized light is applied on a lyotropic liquid crystal, when it is in a nematic phase. Thus, the addition of L-DOPA did not change the phase of the system.

As seen in Fig. 2A, the signal on the left corresponds to the deuterium from L-DOPA-d$_3$ and the signal on the right is from DHO. In Fig. 2B and C, the signal in the middle, near 0 Hz, is from DHO, and the remaining signals are from SDS-d$_{25}$. The separation in Hz between two signals coming from the same deuterium corresponds to the quadrupole splitting ($\Delta\nu_Q$). $\Delta\nu_Q$ can be obtained from the following expression:

$$\Delta\nu_Q = \frac{3CS_{CD}}{4} \tag{1}$$

where C is the quadrupole coupling constant ($C = 170$ kHz in this case[35]), and S_{CD} is the order parameter of a given C–D bond. S_{CD} is obtained from eqn (2):

$$S_{CD} = \frac{\langle 3\cos^2\phi - 1\rangle}{2} \tag{2}$$

here, ϕ is the angle between the C–D bond and the external magnetic field. This term average zero when the C–D bond rotates isotropically, but in anisotropic conditions, such as given by oriented bicelles, $\Delta\nu_Q$ become different from zero. Also $\Delta\nu_Q$ is zero for a C–D bond oriented at the magic angle relative to the magnetic field. Therefore, from all the deuterium atoms present in the amphiphiles that form the bicelle, all of them with the same orientation, those more aligned with the field will produce higher $\Delta\nu_Q$. Also, two deuteriums with the same average orientation will produce different $\Delta\nu_Q$ if they have different amplitudes of oscillation. Thus, $\Delta\nu_Q$ depends on both, the average orientation and dynamics of the C–D bond. Considering these results, and observing the absence of $\Delta\nu_Q$ in the ^{2}H-NMR spectrum of L-DOPA-d$_3$ (Fig. 2A), it can be concluded that either L-DOPA does not establishes an interaction with the aggregate or it is to weak to be oriented by it to produce a $\Delta\nu_Q$.

Table 1 shows $\Delta\nu_Q$ of SDS-d$_{25}$ of systems 1 and 2. In both systems, $\Delta\nu_Q$ decreases as the carbons of SDS-d$_{25}$ get closer to the hydrophobic core. This is expected because the orientational order given by the interface interaction decrease towards the hydrophobic core. The addition of L-DOPA has an effect in the dynamics of the first 8 carbons of SDS, as can be observed in Table 1; $\Delta\nu_Q$ of system 2 decrease around 2 kHz respect to system 1. For the rest of the carbons, the change in $\Delta\nu_Q$ is not significant. These observations imply that L-DOPA must be interacting with the interface of the aggregate without reaching the hydrophobic core. Moreover, considering that Fig. 2A indicates that L-DOPA remains in the isotropic domain of the systems, the interaction with hydrophobic core, if exist, must be too weak to be detected.

Other possible explanation for the decrease in $\Delta\nu_Q$ when L-DOPA is added, is that L-DOPA could affect the system inducing macroscopic changes in the aggregates that affects macroscopic measurements, such as viscosities. An increment in viscosity could explain the widening of the ^{2}H-NMR signals from spectra in Fig. 2B with respect to Fig. 2C, and the decrease in $\Delta\nu_Q$ is given by a lost of orientation of the complete aggregate.[21,22] To check for this phenomena a study on the effects of L-DOPA in other lyotropics nematic systems, approaching the sensitivity of these kind of systems, is added in ESI, Section 1 (Fig. S1†). Unfortunately, since the concentration of added L-DOPA (7.5 mg per ml of water) is saturating, conducting a study similar to those exposed in the ESI Section 1,† is not viable because increasing the concentration of L-DOPA in this systems will produce precipitation, so no phase change could be observed.

3.2 Equilibrium molecular dynamics

To determine if our molecular models is capable to recover the experimentally bicelle dynamics, we rely on the calculations of
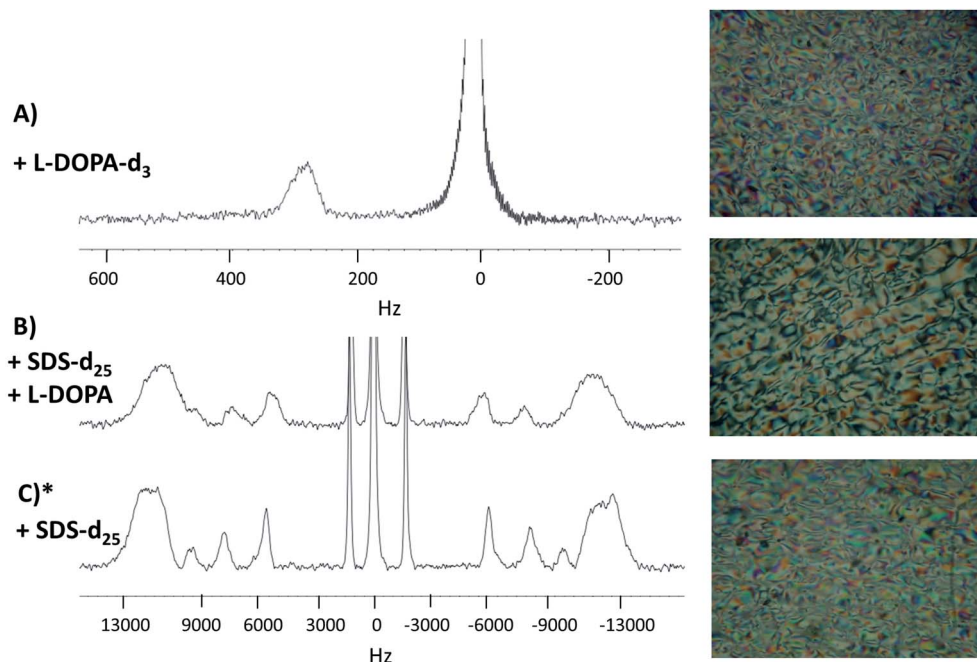
Fig. 2 ^{2}H-NMR spectra and the PLM textures. Panel (A), L-DOPA-d$_3$ in system 2. Panel (B), SDS-d$_{25}$ in system 2. Panel (C), SDS-d$_{25}$ in system 1. * System 1 spectrum and PLM texture were obtained in a previous work and are reproduced with permission from ref. 27.

Table 1 $\Delta\nu_Q$ of systems 1 and 2. * Reproduced with permission from ref. 27

	$\Delta\nu_Q$ (Hz)	
Carbon	System 1*	System 2
1	24 402	22 621
2	24 402	22 621
3	24 402	22 621
4	24 402	22 621
5	24 402	22 621
6	24 402	22 621
7	24 402	22 621
8	24 402	22 621
9	19 470	20 924
10	16 080	15 352
11	11 714	11 225
12	2967	2788

charges of the experimental system in order to compensate for the absence of polarizability. As proposed in the literature, this change corrects the overestimation of the electrostatics interactions that is present in common MD force fields.[36–42]

During simulation of both Box 2 and Box 3, L-DOPA establish a dynamic process, passing from the bulk aqueous phase to interact with the interface of the aggregate (Fig. S2†). These fast L-DOPA exchange denotes a weak interaction with the bilayer: there is a cumulative loss of 115 kJ mol^{-1} of short range LJ and coulombic interaction energy when L-DOPA is transferred from bulk to the surface of the bicelle (see Table S2 at the ESI†). Notably, this energy loss shown by our MD simulations is in agreement with ^{2}H-NMR results (Fig. 2A) explaining why L-DOPA interaction with the bicelle is too weak to produce a $\Delta\nu_Q$.

$\Delta\nu_Q$. For this purpose, we use the order parameter of the C–D bond of DS$^-$ with respect to the direction of the magnetic field applied (xy plane). As observed in Fig. 3, the first five C–D bond splittings are correctly reproduced by the MD simulation of Box 2. Despite the disagreement from carbon 7 to 11, the experimental and simulated values of $\Delta\nu_Q$ are similar. The general trend of the experimental $\Delta\nu_Q$ are well reproduced by the calculation, suggesting that the general dynamics behavior of the simulated bilayer mostly reflects that of the experimental aggregate.

Individual $\Delta\nu_Q$ values can be seen in Table S1 of the ESI.† Importantly, the reproduction of the experimental $\Delta\nu_Q$ was achieved using a temperature of 328 K and halving the DS$^-$
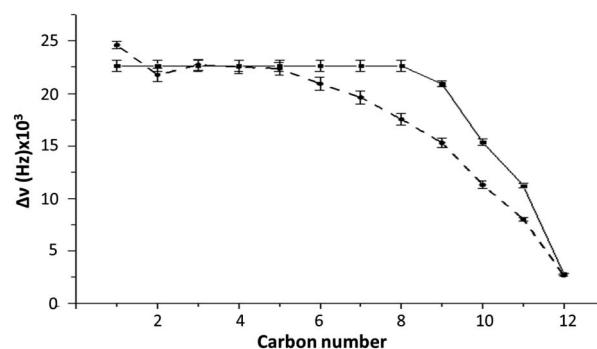

Fig. 3 Comparison of $\Delta\nu_Q$ between experiment (system 2) (continuous line) and MD simulations (Box 2) (dashed line) as a function of the carbon number. Error bars represent the standard deviation. See Table S1† for exact numbers.

Fig. 4 shows the distance, between the center of mass of the bilayer and the center of mass of the TTA$^+$ molecules leaving the bilayer, as a function of simulation time in boxes 1, 2 and 3. These data indicates that adding two L-DOPA (Fig. 4, Panel B) to the system, apparently do not perturb the exchanges dynamic of TTA$^+$ between the bulk and the bicelle. As noted, the addition of two L-DOPA do not change significantly the time that TTA$^+$ molecules remain in the bulk after leaving the bicelle, neither changes the frequency of TTA$^+$'s insertion and expulsion. When two L-DOPA molecules are added, the time that TTA$^+$ molecules remain in the bulk is on average 65 ns, similar to the average time of 68 ns without L-DOPA. During the simulation without L-DOPA, 14 TTA$^+$ molecules were expelled and 13 were inserted; with two L-DOPA molecules, 13 TTA$^+$ molecules were expelled and inserted along the simulation. Thus, the addition of two L-DOPA molecules do not perturb the exchange dynamics of TTA$^+$, resulting average in 0.72 and 0.74 molecules in the bulk, for systems without L-DOPA and with two L-DOPA, respectively.

However, the addition of 4 L-DOPA molecules (Fig. 4C) increases the number of TTA$^+$ molecules present in the bulk. During the MD simulation, 19 TTA$^+$ molecules were expelled and 18 were inserted, with an average time in the bulk of 87 ns, corresponding to an average of 1.65 TTA$^+$ molecules in the bulk.

To check if TTA$^+$ molecules reach a thermodynamic equilibrium in the bulk (after expulsion from the bilayer), we define an internal order parameter as the inner vector going from the first to the second carbon of TTA$^+$ (Fig. 5), and compare its

behavior in the bulk of our simulations with that of a control simulation where the bilayer is absent. The control simulation consisted of a box of $4 \times 4 \times 4$ nm^3 with 1 TTA$^+$, 1 Cl$^-$ and 2126 molecules of H$_2$O, using the same simulation parameters of Box 2, but executed for 200 ns. Fig. 5 shows the probability distribution of the inner vector angle of TTA$^+$ with respect to the z axis in three different scenarios: bulk TTA$^+$ in Box 2, bulk TTA$^+$ in Box 3 and a TTA$^+$ in the control box. As noted, the angular sampling distributions for all systems resulted similar without statistically significant differences, according to a Kruskal–Wallis non-parametric test, suggesting the achievement of a thermodynamic equilibrium. The same histogram was constructed to evaluate if L-DOPA changes the inner angle distribution of a TTA$^+$ molecule in water (Fig. S7†).

In a thermodynamic equilibrium, the standard free energy of a process depends on the equilibrium constant, according to eqn (3):

$$\Delta G^0 = -RT \ln K_{eq} \tag{3}$$

Assuming that our simulation is an equilibrated system, qualitative information about the insertion/expulsion process could be obtained considering that this equilibrium is properly represented by eqn (4):

$$TTA_{bilayer}{}^+ \underset{insertion}{\overset{expulsion}{\rightleftharpoons}} TTA_{bulk}{}^+ \tag{4}$$

Therefore, ΔG^0 of insertion of a TTA$^+$ molecule can be calculated from eqn (3), assuming that the equilibrium constant K_{eq} can be estimated using the quotient between the amount of TTA$^+$ present in the bilayer and in the bulk. Table 2 summarizes the TTA$^+$ insertion/expulsion events, the average time of TTA$^+$ molecules in the bulk, the average number of TTA$^+$ molecules present in the bulk and the ΔG associated with the TTA$^+$ insertion/expulsion process.

As seen on Table 2, for all simulation boxes both the number of insertion/expulsion events and the average time that TTA$^+$ molecules remain in the bulk are different. However, the ΔG^0
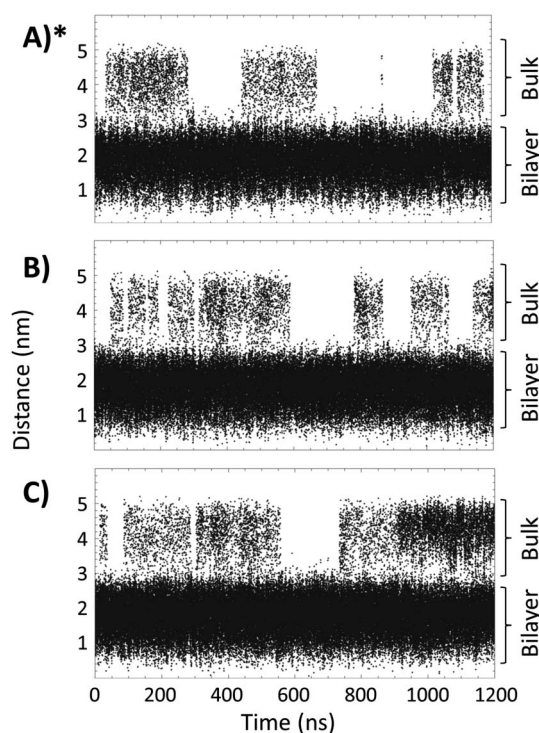

Fig. 4 Distance, as a function of time, between the TTA$^+$ center of mass and the center of mass of the bilayer of the bicelle. Panels (A), (B) and (C), represent Box 1, Box 2 and Box 3, respectively. (*) Reproduced with permission from ref. 27.
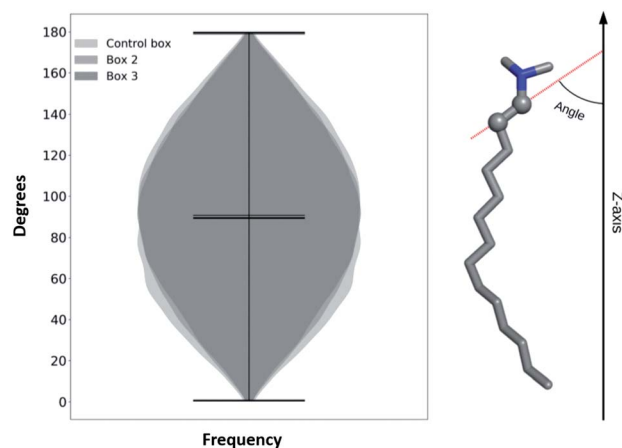

Fig. 5 Histogram of a characteristic inner angle of a TTA$^+$s when are in the bulk solution of Box 2, Box 3 and from 1 TTA$^+$ in water for 200 ns.

Table 2 Data extracted from Fig. 4 and eqn (3)

	Insertion/expulsion events	Avg. time of TTA$^+$ in the bulk (ns)	Avg. number of TTA$^+$ in the bulk	ΔG of insertion (kJ mol^{-1})
Box 1	12/14	68	0.72	−11.00
Box 2	13/14	65	0.74	−10.95
Box 3	18/19	87	1.65	−8.89

calculated according to eqn (3), in all three cases was quite similar, with differences falling within the thermal noise (around 2 kJ mol^{-1}). These ΔG^0 values also support our assumption of thermodynamic equilibrium, suggesting that the presence of L-DOPA will only perturb the kinetics of the TTA$^+$ insertion/expulsion mechanism but not its thermodynamics.

To test the hypothesis of a kinetic effect of L-DOPA on the studied systems, we analyze the autocorrelation function of the order parameters, S_{CH}, of every carbon–hydrogen bond on TTA$^+$. This analysis is computationally expensive because the trajectory must be saved with a higher frequency, to rigorously catch the dynamic behaviour of the atoms. Attending to this cost, we perform the analysis on the control box decribed in the preceding section (one TTA$^+$, one Cl$^-$ in a water box, without the bilayer, simulated for 200 ns) with and without L-DOPA. The autocorrelation curves were fitted to a mono-exponential decay, to obtain the representative τ of the S_{CH} decay of each C–H bond, with and without L-DOPA (Fig. 6), see Table S5† for the exact numbers and Fig. S8† to see the autocorrelation curves. Interestingly, the τ with L-DOPA is significantly shorter than τ without L-DOPA for the first eight carbons. This can be interpreted as an effect of L-DOPA on the dynamics of the C–H bonds, specially for the first carbons that are near the polar head of TTA$^+$. In Table S4† we present the S_{CH} of TTA$^+$ obtained for Box 2, and using a Box containing only water molecules.
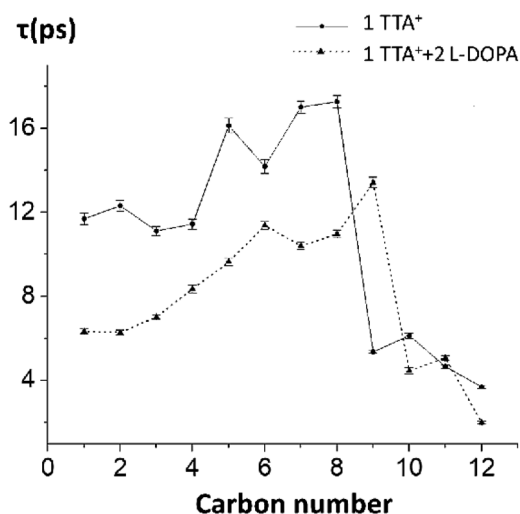

Fig. 6 Representative τ for the mono-exponential decay of autocorrelation function of S_{CH} for each C–H bond in TTA$^+$, with and without L-DOPA. These values were obtain from the simulation of the box containing only water, TTA$^+$ and a Cl$^-$.

3.3 Steered molecular dynamics

To analyze the possible effect of L-DOPA in the thermodynamics of insertion/expulsion mechanism of TTA$^+$ molecules from the bicelle, we performed steered molecular dynamics (SMD) on individual TTA$^+$ molecules belonging to Box 2. To do so, we defined an insertion/expulsion reaction coordinate as the distance in the z-axis from the C12/N atoms of the steered TTA$^+$ molecule with respect to the center of mass of all the N atoms belonging to the proximal TTA$^+$ monolayer. To further determine the influence of L-DOPA on the steered TTA$^+$ molecule, we applied two additional restrictions to keep L-DOPA in the surface of bilayer: a distance restraint to keep it close to the steered TTA$^+$ molecule, and an angular restraint to keep the aromatic ring of L-DOPA parallel to the surface. As a control simulation we performed a similar protocol in the system lacking L-DOPA that was described in ref. 27.

From every simulations we calculate the work performed and then calculate the energy (ΔF) using Jarzynsky equation:

$$\Delta F = -kT \ln \langle \exp^{-W/kT} \rangle \quad (5)$$

Where W is the work and $\langle \rangle$ represent a time-average ensemble over multiple trajectories, T is the temperature and k is the Boltzmann constant. Fig. 7 plots ΔF as a function of time for all studied conditions: insertion and expulsion of TTA$^+$ with and without L-DOPA. As seen for both protocols, insertion and expulsion, ΔF increases in the presence of L-DOPA (Table 3). Notably, the average cost of insertion of one TTA$^+$ molecule in the absence of L-DOPA is 2.77 ± 5.01 kJ mol^{-1}, a value that resulted in the order or the thermal noise, suggesting the spontaneity of this process. The intervention of one L-DOPA molecule increase this energy cost up to 27.90 ± 4.74 kJ mol^{-1}, indicating that the interaction of TTA$^+$ with L-DOPA needs to be broken before the insertion process occurs. It is important to remark that L-DOPA was inserted in the interphase with some restriction as was describe in the last part of Section 2.4.2. These restrictions are much needed because during the insertion/expulsion of the TTA$^+$ under study, is possible that L-DOPA leave the interphase, as is suggested by the loose of 115 kJ mol^{-1} when L-DOPA pass from the bulk to the interphase, as is exposed in Fig. S2.†

Regarding the interaction of L-DOPA with the interphase, Fig. S3† shows an alternative insertion/expulsion mechanism given by the interaction of L-DOPA with the amphiphile molecule that is being inserted or expelled.

To further analyze these results, it is important to address the differences between the energies obtained from the equilibrium MD and the SMD simulation protocols. Free energy
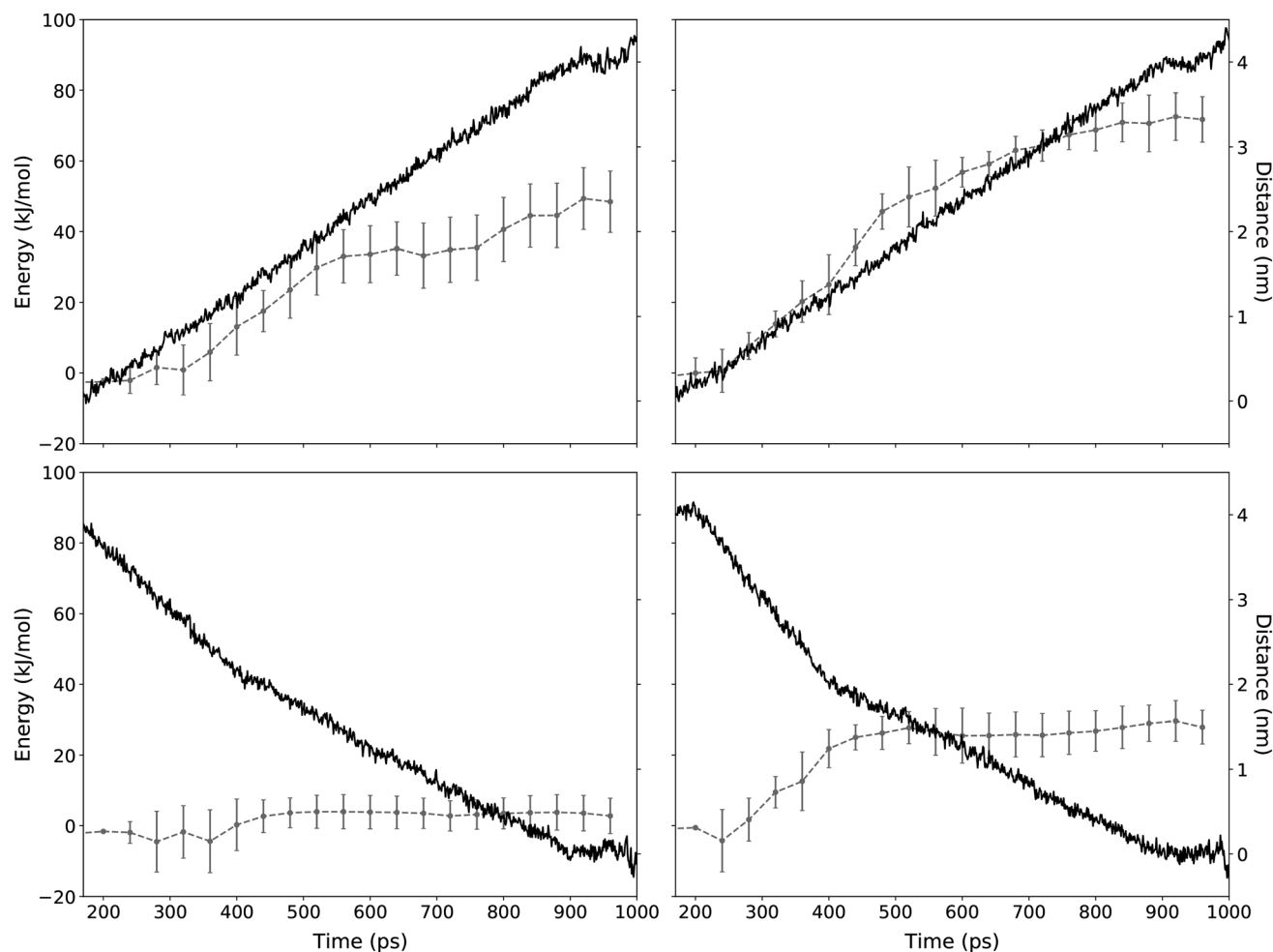
RSC Advances

Paper

Fig. 7 Distance and energy of a TTA$^+$ molecule during the SMD protocol. The application of the SMD protocol simulating the expulsion and the insertion mechanism is presented in the top and bottom panels, respectively. Red line corresponds to the energy as function of simulation time (left y-axis). Left panels shows SMD experiments without L-DOPA and right panels with L-DOPA. Error bars represent the standard deviation of n independent steering experiments for TTA$^+$ molecules according to Table 3 (see Methods). Blue line shows the distance between the steered TTA$^+$ molecule and the rest of the bilayer (right y-axis).

Table 3 Data extracted from Fig. 7 at the last frame of the steered MD protocol. ΔF is the free energy according to eqn (5) and n is the number of successful replicas achieved

		ΔF (kJ mol^{-1})	n
Expulsion	Without L-DOPA	48.45 ± 8.69	48
	With L-DOPA	66.18 ± 7.32	35
Insertion	Without L-DOPA	2.77 ± 5.01	40
	With L-DOPA	27.90 ± 4.74	23

values obtained from equilibrium MD using eqn (3) represent a function of state for a molecular system in a near-to-equilibrium condition: the TTA$^+$ molecules that become expelled from the bicelle describe a conformational sampling in the solvent equivalent to that of TTA$^+$ molecules in solution (Fig. 5).

On the other hand, ΔF values are obtained from the ensemble of trajectories generated by the irreversible work of the SMD protocols executed to either insert or expulse a TTA$^+$ molecule from the bilayer. Therefore, the SMD protocol assume an out of equilibrium condition where irreversible work is performed between the two states: a TTA$^+$ molecule embedded in the bilayer and its counterpart embedded in the solvent. As a consequence, these energies can not be compared directly as they represent different thermodynamic processes.

However, ΔF implies that the balance between the insertion and the expulsion process, considered as a whole, is tilted towards the insertion and, as we increase the concentration of L-DOPA, the cost of the insertion process increases, an observation that is in agreement with the increase of ΔG shown in Table 2.

Likewise, SMD results are useful to better describe the "dive in mechanism" of TTA$^+$ molecules.[27] Thus, in the absence of L-DOPA, the ΔF of expulsion of a TTA$^+$ molecule is more than 17 times higher than the value of its ΔF of insertion, the latter being near to thermal noise. This is a clue about how energetically costly is the expulsion mechanism of an amphiphile from

its aggregate, compared to that of the insertion value. Notably, this observation in agreement with the spontaneity of the insertion process denoted by ΔG values in Table 2. It is important to remark that L-DOPA was inserted in the interphase with some restriction as was describe in the last part of Section 2.4.2. These restrictions are much needed because during the insertion/expulsion of the TTA$^+$ under study, is possible that L-DOPA leave the interphase, as is suggested by the loose of 115 kJ mol^{-1} when L-DOPA pass from the bulk to the interphase, as is exposed in Fig. S2.†

Even more interesting is the apparent contradiction between the values of ΔF and ΔG when L-DOPA is added. In SMD, both cases, expulsion and insertion, have a 20 kJ mol^{-1} increase in ΔF compared to condition without L-DOPA (Table 3). To better comprehend these results, it should keep in mind that the ΔG from equilibrium MD implies both process simultaneously, insertion and expulsion. Instead SMD considers both process independently. In SMD with L-DOPA both process have a similar increase in energy, so both increases are canceled when they are considered together, because they act in opposite sides of the eqn (4). As whole, our data supports the notion that adding L-DOPA will affect the kinetic of the "dive in mechanism" rather than its thermodynamics.

4 Conclusions

Previously, it have been shown that TTA molecules have an equilibrium between the bilayer and the bulk, when placed in a bilayer with TTA$^+$ as the main component.[27] The bilayer simulated (Box 2) reproduce the dynamics of the bicelles that form the lyotropic nematic liquid crystal (system 2), see Fig. 2.

NMR analysis shows that L-DOPA does not seems to significantly affect overall TTA$^+$ bicelle dynamic properties (see Fig. 2) but it affects the exchange kinetic of TTA$^+$ between bulk and bilayer. Simulation experiments support this conclusion because L-DOPA do not change ΔG^0 (see Table 2). L-DOPA affects the autocorrelation time of C–H order parameters from TTA$^+$ chain, which are related with the re-orientational order of the carbon chain of these molecules (see Fig. 6). These evidences suggest that L-DOPA intervenes in the kinetic of the dive in mechanism, but deeper analysis are required to known the exact mechanism.

It is interesting that the L-DOPA affects the kinetics of the process without affecting its thermodynamics. There is a kind of robustness in the TTA$^+$'s insertion/expulsion equilibrium that was not expected, considering the intervention of L-DOPA. SMD experiments support this conclusion and favors kinetic perturbation.

Bicelles with TTA$^+$ as main component, are interesting models of potential new drug delivery systems. This work contributes to the understanding of how a pharmacological interesting molecules like L-DOPA affects the dynamic properties of a bilayer.

Conflicts of interest

There are no conflicts to declare.

References

1 D. Elgueta, M. S. Aymerich, F. Contreras, A. Montoya, M. Celorrio, E. Rojo-Bustamante, E. Riquelme, H. González, M. Vásquez, R. Franco, *et al.*, *Neuropharmacology*, 2017, **113**, 110–123.

2 Y. Z. Zhou, R. G. Alany, V. Chuang and J. Wen, *Chromatographia*, 2012, **75**, 597–606.

3 T. Tahvanainen and A. Haraguchi, *Eur. J. Soil Biol.*, 2013, **54**, 41–47.

4 K. J. Black, J. L. Carl, J. M. Hartlein, S. L. Warren, T. Hershey and J. S. Perlmutter, *J. Neurosci. Methods*, 2003, **127**, 19–29.

5 N. Ngwuluka, V. Pillay, L. C. Du Toit, V. Ndesendo, Y. Choonara, G. Modi and D. Naidoo, *Expert Opin. Drug Delivery*, 2010, **7**, 203–224.

6 S. Tang, L. J. Martinez, A. Sharma and M. Chai, *Org. Lett.*, 2006, **8**, 4421–4424.

7 P. Gambaryan, I. Kondrasheva, E. Severin, A. Guseva and A. Kamensky, *Exp. Neurol.*, 2014, **23**, 246–252.

8 C. R. Sanders and J. Prestegard, *Biophys. J.*, 1990, **58**, 447–460.

9 G. Scalia, *ChemPhysChem*, 2010, **11**, 333–340.

10 D. Vijayaraghavan, *J. Mol. Liq.*, 2014, **199**, 128–132.

11 M. Casavant, D. Walters, J. Schmidt and R. Smalley, *J. Appl. Phys.*, 2003, **93**, 2153–2156.

12 A. Takai, Y. Yamauchi and K. Kuroda, *J. Am. Chem. Soc.*, 2009, **132**, 208–214.

13 S. Warren and U. Wiesner, *Pure Appl. Chem.*, 2009, **81**, 73–84.

14 X. Zhang, W. Lu, J. Dai, L. Bourgeois, J. Yao, H. Wang, J. R. Friend, D. Zhao and D. R. MacFarlane, *Sci. Rep.*, 2014, **4**, 7420.

15 S. Che, Z. Liu, T. Ohsuna, K. Sakamoto, O. Terasaki and T. Tatsumi, *Nature*, 2004, **429**, 281–284.

16 H. Lin and C. Mou, *Acc. Chem. Res.*, 2002, **35**, 927–935.

17 S. Umadevi, H. Lee, V. Ganesh, X. Feng and T. Hegmann, *Liq. Cryst.*, 2014, **41**, 265–276.

18 V. Bahamonde-Padilla, J. López-Cascales, R. Araya-Maturana, M. Martínez-Cifuentes and B. Weiss-López, *ChemPhysChem*, 2014, **15**, 1422–1431.

19 U. H. Durr, M. Gildenberg and A. Ramamoorthy, *Chem. Rev.*, 2012, **112**, 6054–6074.

20 D. E. Warschawski, A. A. Arnold, M. Beaugrand, A. Gravel, É. Chartrand and I. Marcotte, *Biochim. Biophys. Acta, Biomembr.*, 2011, **1808**, 1957–1974.

21 A. Ruiz-Fernández, J. López-Cascales, J. Giner-Casares, R. Araya-Maturana, F. Díaz-Baños, D. Muñoz-Gacitúa and B. Weiss-López, *RSC Adv.*, 2016, **6**, 7455–7464.

22 A. Ruiz-Fernández, J. López-Cascales, J. Giner-Casares, R. Araya-Maturana, F. Díaz-Baños and B. Weiss-López, *RSC Adv.*, 2016, **6**, 85411–85419.

23 H. K. Bisoyi and S. Kumar, *Chem. Soc. Rev.*, 2010, **39**, 264–285.

24 L. Mäler and A. Gräslund, *Macromolecular Drug Delivery*, Springer, 2009, pp. 129–139.

25 C. Müller-Goymann, *Eur. J. Pharm. Biopharm.*, 2004, **58**, 343–356.

26 C. Kang, C. G. Vanoye, R. C. Welch, W. D. Van Horn and C. R. Sanders, *Biochemistry*, 2010, **49**, 653–655.

27 A. Ruiz-Fernández, *J. Phys. Chem. C*, 2018, **122**, 1192–1196.

28 G. A. Tribello, M. Bonomi, D. Branduardi, C. Camilloni and G. Bussi, *Comput. Phys. Commun.*, 2014, **185**(2), 604–613.

29 G. Raffard, S. Steinbruckner, A. Arnold, J. H. Davis and E. J. Dufourc, *Langmuir*, 2000, **16**, 7655–7662.

30 L. S. Vermeer, B. L. De Groot, V. Réat, A. Milon and J. Czaplicki, *Eur. Biophys. J.*, 2007, **36**, 919–931.

31 M. Bloom, J. H. Davis and A. L. Mackay, *Chem. Phys. Lett.*, 1981, **80**, 198–202.

32 K. Merz, B. Roux and B. Membranes, *A Molecular Perspective from Computation and Experiment*, Birkhäuser, Boston, 1996.

33 M. Brown, R. Thurmond, S. Dodd, D. Otten and K. Beyer, *J. Am. Chem. Soc.*, 2002, **124**, 8471–8484.

34 K. Hiltrop, *Lyotropic liquid crystals in topics in physical chemistry*, Springer New York, 1994, vol. 3.

35 A. Seelig and J. Seelig, *Biochemistry*, 1974, **13**, 4839–4845.

36 B. Jonsson, O. Edholm and O. Teleman, *J. Chem. Phys.*, 1986, **85**, 2259–2271.

37 E. Egberts, S. Marrink and H. Berendsen, *Eur. Biophys. J.*, 1994, **22**, 423–436.

38 P. Ahlstrom and H. Berendsen, *J. Phys. Chem.*, 1993, **97**, 13691–13702.

39 J. López Cascales, J. De la Torre, S. Marrink and H. Berendsen, *J. Chem. Phys.*, 1996, **104**, 2713–2720.

40 P. David, W. van Gunsteren and A. Mark, *J. Comput. Chem.*, 2010, **31**, 1117–1125.

41 T. Heinz, W. van Gunsteren and P. Hünenberger, *J. Chem. Phys.*, 2001, **115**, 1125–1136.

42 V. Bahamonde-Padilla, J. Espinoza, B. Weiss-Lopez, J. L. Cascales, R. Montecinos and R. Araya-Maturana, *J. Chem. Phys.*, 2013, **139**, 14703–14711.